LAWRENCE
LIVERMORE
NATIONAL
LABORATORY

LLNL-PROC-694818

Spatial resolution measurements of the Advanced Radiographic Capability X-ray Imaging System at energies relevant to Compton radiography

G. N. Hall, N. Izumi, O. L. Landen, R. Tommasini, J. P. Holder, D. Hargrove, D. K. Bradley, A. Lumbard, J. G. Cruz, K. Piston, J. J. Lee, E. Romano, P. M. Bell, A. C. Carpenter, N. E. Palmer, B. Felker, V. Rekow, F. V. Allen

June 13, 2016

High Temperature Plasma Diagnositcs
Madison, WI, United States
June 5, 2016 through June 9, 2016

Disclaimer

Spatial resolution measurements of the Advanced Radiographic Capability X-ray Imaging System at energies relevant to Compton radiography[a)]

G. N. Hall,[1, b)] N. Izumi,[1] O. L. Landen,[1] R. Tommasini,[1] J. P. Holder,[1] D. Hargrove,[1] D. K. Bradley,[1] A. Lumbard,[1] J. G. Cruz,[1] K. Piston,[1] J. J. Lee,[2] E. Romano,[2] P. M. Bell,[1] A. C. Carpenter,[1] N. E. Palmer,[1] B. Felker,[1] V. Rekow,[1] and F. V. Allen[1]

[1)] *Lawrence Livermore National Laboratory, 7000 East Avenue., Livermore, California 94550*

[2)] *National Security Technologies LLC, 161 S Vasco Rd, Livermore, CA 94551*

Compton radiography provides a means to measure the integrity, ρR and symmetry of the DT fuel in an inertial confinement fusion implosion near peak compression. Upcoming experiments at the National Ignition Facility will use the ARC (Advanced Radiography Capability) laser to drive backlighter sources for Compton radiography experiments, and will use the newly commissioned AXIS (ARC X-ray Imaging System) instrument as the detector. AXIS uses a dual-MCP (micro channel plate) to provide gating and high DQE at the 40–200keV x-ray range required for Compton radiography, but introduces many effects that contribute to the spatial resolution. Experiments were performed at energies relevant to Compton radiography to begin characterization of the spatial resolution of the AXIS diagnostic.

I. INTRODUCTION

Compton radiography provides a means to measure the density and asymmetries of the DT fuel in an inertial confinement fusion capsule near the time of peak compression[1,2]. The AXIS instrument[4] has recently been commissioned at the National Ignition Facility, and will be the detector for Compton radiography driven by the ARC laser[3]. ARC converts a NIF quad into several 1kJ, 30ps beams (4 beams at present, 8 in the future) and will be used to produce Bremsstrahlung X-ray backlighter sources in the range of 40keV to 200keV for Compton Radiography.

AXIS uses a dual-MCP configuration to provide significantly improved detective quantum efficiency (DQE) at high x-ray energies, and to provide gating to reduce background from neutrons and hard x-rays from laser-plasma-interactions in the hohlraum. The dual-MCP system uses a thick, low gain MCP as a volumetric photocathode in a chevron configuration with a thinner, high gain MCP which acts an amplifier. This configuration has demonstrated a DQE of ∼4.5% at 60keV[5] compared to a DQE of ∼1.1% for a single MCP with the same overall gain. This enables AXIS to provide a cleaner image that will allow the density and distribution of the compressed DT fuel to be measured with significantly greater accuracy as ICF experiments are tuned for ignition.

In order to measure the density of the DT fuel to the required accuracy, it is important to know the resolution of the AXIS diagnostic at energies relevant to Compton radiography experiments. Use of a chevron configuration at high x-ray energies introduces many effects that contribute to the spatial resolution of the instrument. High energy X-rays produce detection events throughout the volume of both MCPs, crossing many pores, and the gaps between the MCPs and between the MCP and the phosphor allow for the transverse spread of electrons.

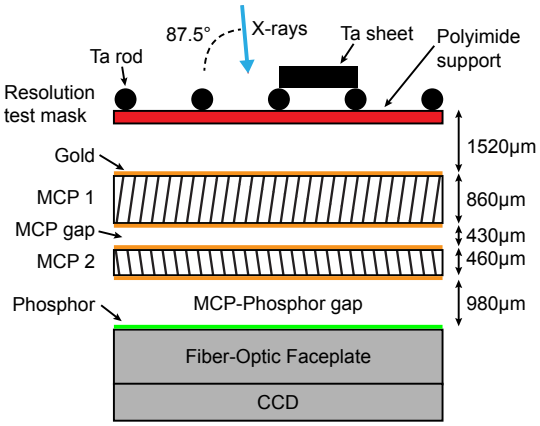

FIG. 1. Top down view of the experimental setup. The pore bias of each MCP is in the horizontal plane.

Here we present measurements of the spatial resolution of AXIS in DC mode at 4 x-ray energies between 20keV and 100keV.

II. EXPERIMENTAL SETUP AND ANALYSIS

These measurements were performed at the High Energy X-ray (HEX) laboratory[6] at National Security Technologies LLC, a source capable of producing x-ray energies relevant to Compton radiography. The HEX generates characteristic fluorescence lines in the range 8keV to 111keV, and can provide continuous x-ray intensities on the order of 10^6 photons per second per cm^2. The HEX was operated with four different fluorescer materials (Ag, W, Bi, U) and appropriate filters such that the spectrum was dominated by the Kα lines of each material at 22keV,

[a)] Contributed paper published as part of the Proceedings of the 20th Topical Conference on High-Temperature Plasma Diagnostics, Atlanta, Georgia, June, 2014.

[b)] Author to whom correspondence should be addressed: hall98@llnl.gov.

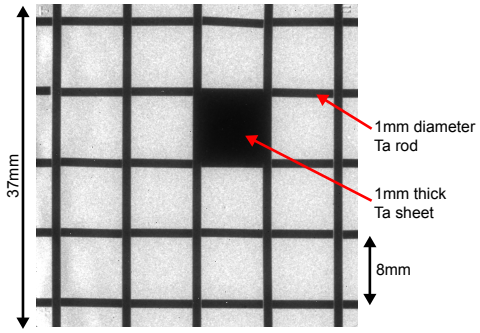

FIG. 2. An example AXIS image at 59keV with the resolution mask. The center-to-center distance of the rods is 8mm.

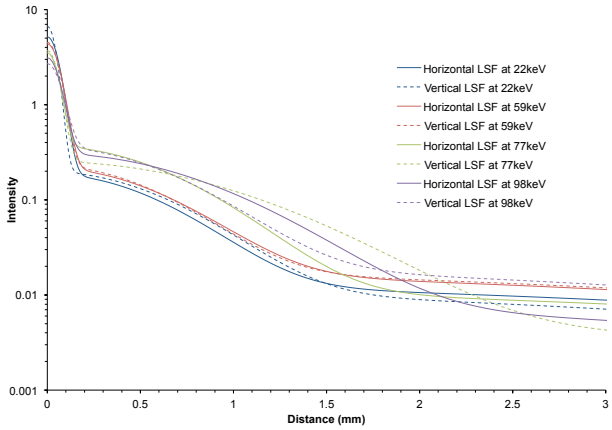

FIG. 3. Vertical and horizontal LSFs at 4 x-ray energies.

59keV, 77keV and 98keV.

In the experimental setup, shown in Fig.1, the full area of AXIS was exposed to x-rays incident at 87.5° in the horizontal plane to reproduce the angle of incidence on a Compton radiography experiment. A resolution test mask, shown in an example AXIS image in Fig.2, was placed ∼1.5mm in front of AXIS and consisted of a grid of 1mm diameter rods of Ta, with one grid square covered by a 1mm thick Ta sheet. The advantage of using rods rather than a knife edge is that a cylindrical object requires no alignment relative to the x-ray source and the transmission through it can be modeled analytically.

AXIS was operated in DC mode, as the x-ray intensity was insufficient for pulsed mode, at all 4 energies both with and without the resolution mask in place. On NIF experiments a film will be used to record the images, but for these experiments a CCD was used.

An optimization routine is used to calculate a horizontal and vertical line spread function (LSF) for AXIS at each of the 4 energies. Firstly, the image with the resolution grid is divided by an image without the grid to produce an image of the transmission, and a lineout is taken across a feature of the resolution mask. The transmission of x-rays through the region sampled by the lineout is calculated and then convolved with an initial guess of the LSF to produce a model lineout. The model lineout is then compared to the real lineout and the residual calculated. The optimization routine then modifies the LSF iteratively until the residual between the real and modeled lineout is minimized. The end result is the best estimate of the actual LSF.

For this process, a function consisting of three Gaussians is chosen to represent the LSF. The ease of analytical manipulation of the Gaussian functional form was advantageous for analysis, and three terms was the minimum number required to obtain a satisfactory fit to the data. The form of the fit LSF is:

$$LSF = A_1 e^{-x^2/2\sigma_1} + A_2 e^{-x^2/2\sigma_2} + A_3 e^{-x^2/2\sigma_3} \quad (1)$$

The optimization routine was constrained such that $\sigma_3 > \sigma_2 > \sigma_1$ to give a long, medium and short range component, and A_n was constrained such that the area under the LSF was unity.

Analysis of different regions of the resolution mask were used to improve the accuracy of the LSF fit. First, the Ta slab section of the mask was analyzed. The slab is sufficiently wide to observe the manner in which the signal decreases almost to zero without interference from short and medium-range effects. This allows the long range component of the LSF to be measured more accurately, and by running the optimization routine on multiple lineouts taken across the slab, the mean value of A_3 and σ_3, and the standard deviation of each, is found. Then, every rod feature in the image is analyzed with the values of A_3 and σ_3 only being allowed to vary within 2 standard deviations of the mean values found during the slab analysis. This produces mean vales and standard deviations for A_1, A_2, σ_1 and σ_2.

III. RESULTS AND DISCUSSION

The LSF, shown in Fig.3 varies as a function of both x-ray energy and direction. Fore each energy and direction, Fig.4 shows the FWHM and contribution to the LSF for each of the short, medium and long-range Gaussian components. It should be noted that the error bars are much larger for the 77keV and 98keV measurements because the filtering required to produce a clean spectrum dominated by Kα lines at these energies reduced the x-ray intensity dramatically. As a result, the signal level in the 77keV and 98keV images is only ∼1% of the signal level in the 22keV and 59keV images, resulting in substantially more noise and error bars that are many times larger.

The short, medium and long-range FWHMs are useful for building a picture of the physical processes underlying each component.

Several effects are likely to contribute to the short-range component shown in Fig.3a, but the dominant effect is likely the transverse spread of electrons in the gap between the two MCPs, and also in the gap between the

MCP and the phosphor. Wiedwald et al[7] describe measurements of the initial transverse energy of electrons between an MCP and phosphor in the direction perpendicular and parallel to the pore bias direction as a result of the electric field in the gap acquiring a component in the direction of the pore bias. For an MCP in DC mode with a pore bias of 5° (similar to the 8° bias of the AXIS MCPs) this energy was measured to have a mean value of 1eV and 2.4eV in the perpendicular and parallel directions respectively. For a chevron MCP arrangement, it might be expected that the perturbation to the electric field from the upper and lower MCPs would cancel out in the gap between them, leaving the perpendicular and parallel transverse energies equal at ∼1eV. In the gap between the MCP and phosphor of a chevron arrangement however, the transverse energies should be as measured by Wiedwald et al. Using the spacings and voltages specified in Fig.1 for the MCP gap and assuming 1eV in both directions, the spread is expected to be ∼94μm. For the phosphor gap, 1eV in the vertical direction and 2.4eV in the horizontal direction will produce a spread of ∼70μm and ∼108μm respectively. Added in quadrature, this gives ∼117μm in the vertical direction and ∼143μm in the horizontal.

A second effect on the short range component is the range of the primary electron, generated predominantly by photoionisation of the Pb dopant within the MCP glass. For 22keV, 59keV and 77keV x-rays, 76% of the primary electrons are from photoionization from the Pb L-shell, resulting in primary electrons with 7keV, 44keV and 62keV respectively. For the 98keV x-rays, 79% of photoelectrons are ionized from the Pb K-shell and have an energy of 10keV. The mean range of these primary electrons in the AXIS MCPs is expected to be ∼2μm, ∼14μm, ∼26μm and ∼1μm for the 22keV, 59keV, 77keV and 98keV x-rays respectively.

Lastly, the effect of x-rays crossing multiple pores should be considered. For all the x-ray energies used in these experiments, the MCPs can be considered optically thin. Therefore, photoelectric events will occur throughout the entire volume, but for gains >1 shallow events will contribute more to the final signal than deep events. For an MCP operating with gain G, the fraction of the plate thickness that contributes to the final signal is ∼1/ln(G). AXIS operates MCP1 with a gain of ∼10, meaning that only the first ∼43% of the plate thickness contributes to the signal. The x-rays are incident at 10.5° to the pores of MCP1, resulting in a ∼157μm horizontal displacement as the x-rays traverse the plate. Assuming only the first ∼43% of MCP1 contributes to the signal, this effect is expected to produce an additional horizontal spread of ∼68μm.

Adding these effects in quadrature for the vertical direction gives 136μm, 139μm, 145μm and 136μm for 22keV, 59keV, 77keV and 98keV x-rays respectively, which is within the error of the measured values for all energies except 22keV. In the horizontal direction the quadrature sum gives 158μm, 161μm, 166μm and 158μm

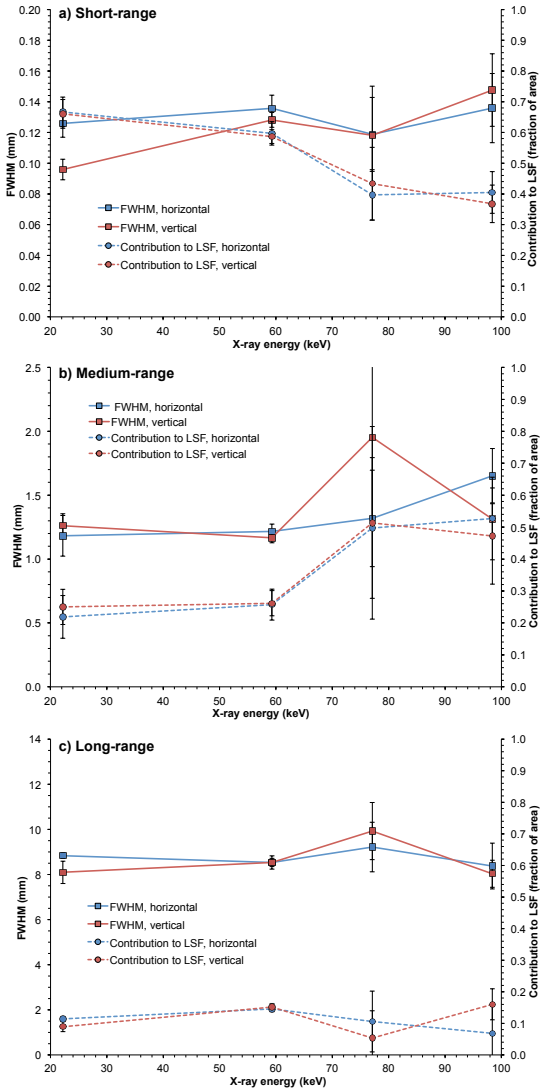

FIG. 4. The FWHM and contribution to the LSF (as a fraction of the area) of the a) short, b) medium and c) long-range Gaussian components.

for 22keV, 59keV, 77keV and 98keV x-rays respectively, which is slightly above the measured values for all energies except 98keV. It is possible that the direction of the pore bias in MCP2, which would translate the signal in the opposite horizontal direction to the pore bias in MCP1, could be responsible for the actual horizontal FWHM being lower than the estimate above.

The medium-range component, shown in Fig.3b, could be due to visible photons emitted from the phosphor into the gap being reflected back from the gold coated rear surface of MCP2. It is expected that this effect would occur on scale lengths similar to the ∼1mm MCP-phosphor gap. Alternatively, the medium range component could be due to Compton scattering of incident x-rays from the Ta rods comprising the resolution mask. Using the Klein-Nishina formula to calculate the probability of scattering over an angular range from 0° to 90° from the incident

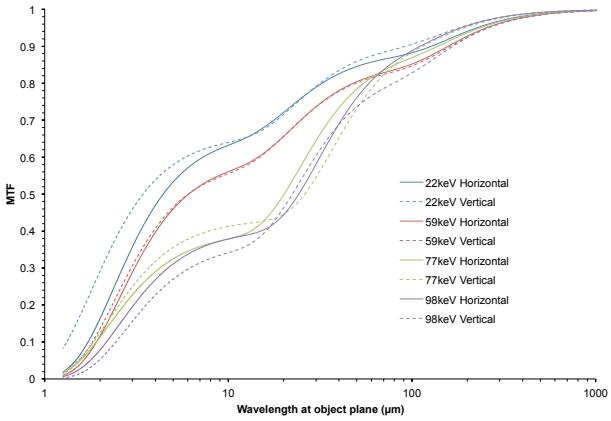

FIG. 5. 1D vertical and horizontal MTFs at 4 x-ray energies.

angle (i.e. angles where the scattered photon can still hit the MCP) gives the mean scattering angle as 36°–38° for 22keV–98keV. The most likely region of a rod to produce scattering that will eventually be detected by the MCP is the region near the lateral edges, i.e. close to the surface of the rod ∼1.5mm above MCP1. Photons will arrive at this region with minimal likelihood of already having been absorbed by the rod, and can continue onwards with minimal likelihood of being absorbed. A photon scattered from ∼1.5 above the surface of MCP1 at 37° will be deflected up to ∼1.1mm in a direction perpendicular to the rod, which closely matches the FWHM of the medium-range component. If scattering is indeed the responsible mechanism then this component will be independent of the detection device: an upcoming experiment will repeat this measurement with an image plate to address this question.

The long-range component, shown in Fig.3c. Its lack of x-ray energy dependance and its very long FWHM suggests that it might be due to electrons incident on the phosphor undergoing elastic scattering in the transverse direction. Multiple scattering events can result in electrons traveling a long transverse distance in the gap.

LSFs were used to calculate 1D modular transfer functions (MTF) at the object plane as a function of wavelength for an imaging system with magnification of 100, the magnification of the Compton radiography platform on NIF, and are shown in Fig.5.

IV. CONCLUSIONS

The AXIS instrument is a gated detector that has recently been commissioned on the National Ignition Facility as the detector for Compton radiography. AXIS uses a dual-MCP configuration that results in improved DQE at high x-ray energies, but limits the spatial resolution of the detector. The spatial resolution of AXIS was characterized at 22keV, 59keV, 77keV and 98keV in DC mode in both the horizontal and vertical directions. Line spread functions were fitted using a combination of 3 Gaussians, and the 1D modular transfer function was calculated for the horizontal and vertical direction at each energy.

ACKNOWLEDGMENTS

Lawrence Livermore National Laboratory is operated by Lawrence Livermore National Security, LLC, for the U.S. Department of Energy, National Nuclear Security Administration under Contract No. DE-AC52-07NA27344. (LLNL-JRNL-555712)

[1]R. Tommasini et al, Rev. Sci. Instrum. 79, 10E901 (2008).
[2]R. Tommasini et al, Phys. Plasmas 18, 056309 (2011).
[3]J. K. Crane et al, J. Phys.: Conf. Ser. 244, 032003 (2010).
[4]G. N. Hall et al, Rev. Sci. Instrum. 85, 11D624 (2014)
[5]N. Izumi et al, Rev. Sci. Instrum. 85, 11D623 (2014)
[6]J. J. Lee et al, Proc. SPIE 8505, 850508 (2012)
[7]J. D. Wiedwald et al, SPIE 1346, 449 (1990)